Available online at www.sciencedirect.com

ScienceDirect

Procedia Engineering 133 (2015) 688 – 697

Procedia Engineering

www.elsevier.com/locate/procedia

6th Fatigue Design conference, Fatigue Design 2015

Thermo-Mechanical Finite Element Simulation and Fatigue Life Assessment of a Copper Mould for Continuous Casting of Steel

Jelena Srnec Novak[a]*, Denis Benasciutti[a], Francesco De Bona[a], Aleksandar Stanojević[b], Patrik Huter[b]

[a]*DIEGM, University of Udine, Via delle Scienze 206, Udine 33100, Italy*
[b]*Chair of Mechanical Engineering, Montanuniversität Leoben,Franz Josef-Straße 18, Leoben 8700, Austria*

Abstract

This work describes the thermo-mechanical analysis of a copper mould for continuous steel casting. During the process, the molten steel passes through a water cooled mould. The inner part of the component is subjected to a huge thermal flux. Consequently large temperature gradients occur across the component, especially in the region near to the meniscus, and cause elastic and plastic strains. The aim of this work is to set up an industrially oriented approach to assess the fatigue life of the copper mould. To achieve the goal, a three-dimensional finite element model is analyzed in dependence of four different material models (linear kinematic hardening, combined, stabilized and accelerated material model). The main question is which material model is more suitable to be used. Material coefficients for all applied material and fatigue life models are estimated from experimental, isothermal low cycle fatigue data. The fatigue life is also assessed depending on different material models. The results obtained with the FEM analysis are examined and compared.

© 2015 Published by Elsevier Ltd. This is an open access article under the CC BY-NC-ND license (http://creativecommons.org/licenses/by-nc-nd/4.0/).
Peer-review under responsibility of CETIM

Keywords: copper mould, thermo-mechanical analysis, cyclic plasticity, material models, fatigue assessment

* Corresponding author. Tel.: +39-(0)432-558297; fax: +39-(0)432-558251.
E-mail address: jelena.srnec@uniud.it

1877-7058 © 2015 Published by Elsevier Ltd. This is an open access article under the CC BY-NC-ND license (http://creativecommons.org/licenses/by-nc-nd/4.0/).
Peer-review under responsibility of CETIM
doi:10.1016/j.proeng.2015.12.651

1. Introduction

The work describes the thermo-mechanical analysis of a copper mould used in the continuous casting process. The mould is that part of the steelmaking plant where the molten steel is cooled and first shaped. The high temperature of the molten steel causes thermal fluxes and temperature gradients in the component. As a result, considerable stresses and plastic strains are induced, which leads to deformations and thermal cracks at the inner surface [1]. A mould without cracks and with close dimensional tolerance contributes to safety in the working process and quality of the final product [2].

The aim of this work is to set up an industrially oriented approach to assess the fatigue life of the copper mould. A thermo-mechanical analysis with a three-dimensional finite element model is performed to compute stress-strain distribution. Mechanical analyses are done with different types of elasto-plastic material models. The main reason for using different material models was to investigate the correlation between material models and fatigue life assessment. Many types of material models have been developed and described in the literature until now. With increasing complexity of the material model, the numbers of needed material parameters increase as well. Material parameters are estimated from experimental data. For some models (e.g. linear kinematic hardening model), material parameters can be estimated using data obtained simply by a tensile test, while for other models (e.g. nonlinear kinematic and isotropic hardening models) it is necessary to use data obtained by low cycle fatigue (LCF) tests. It is important to note that with increasing complexity of the material model the computation time and numerical effort also increases.

Nomenclature

q	thermal flux	e	speed of stabilization
q_{max}	maximum thermal flux	E_1	Young's modulus – tensile portion of the first hysteresis loop
$\boldsymbol{\sigma}'$	stress deviator tensor		
$\boldsymbol{\alpha}'$	back stress deviator tensor	E_s	Young's modulus – stabilized loop
σ_0	initial yield stress	σ'_f	fatigue strength coefficient
σ_{0*}	actual yield stress	b	fatigue strength exponent
σ_a	stress amplitude	ε'_f	fatigue ductility coefficient
ε_a	strain amplitude	c	fatigue ductility exponent
ε_{pl}	plastic strain	N_f	number of cycles to failure
$\varepsilon_{pl,a}$	plastic strain amplitude	σ_{uts}	ultimate tensile strength
$\varepsilon_{pl,acc}$	accumulated plastic strain	D	ductility
C	initial hardening modulus	$\Delta\varepsilon$	strain range
C_{lin}	initial hardening modulus (Prager's rule)	$\Delta\varepsilon_{el}$	elastic strain range
γ	nonlinear recovery parameter	$\Delta\varepsilon_{pl}$	plastic strain range
R	drag stress	$\Delta\varepsilon_{eq}$	equivalent strain range
R_∞	saturation value	$\varepsilon_1, \varepsilon_2, \varepsilon_3$	principal strains in 1,2,3 direction
N	number of cycles		

2. Description of the component

A mould is a part of the continuous casting line where solidification of the steel starts. The mould geometry is a long "cylinder" with a hollow square cross section. The molten steel flows from the upper part of the mould to the bottom part where the steel exits with a thin solidified shell. During the solidification of the steel, a huge thermal flux, q, passes from the molten steel to the inner surface of the mould, which is then subjected to high temperatures. The thermal flux varies between two conditions: when the plant is switched on the thermal flux increases until reaching the maximum value q_{max}, while thermal flux is absent once the plant is switched off, see Fig. 1. The outer mould surface is cooled by water. The upper part of the mould is hung to a surrounding steel frame with no

additional imposed mechanical constrain. A mould is usually made of copper alloys because of their high conductivity that helps the solidification of the steel. The mould considered in this study is made of CuAg-alloy.

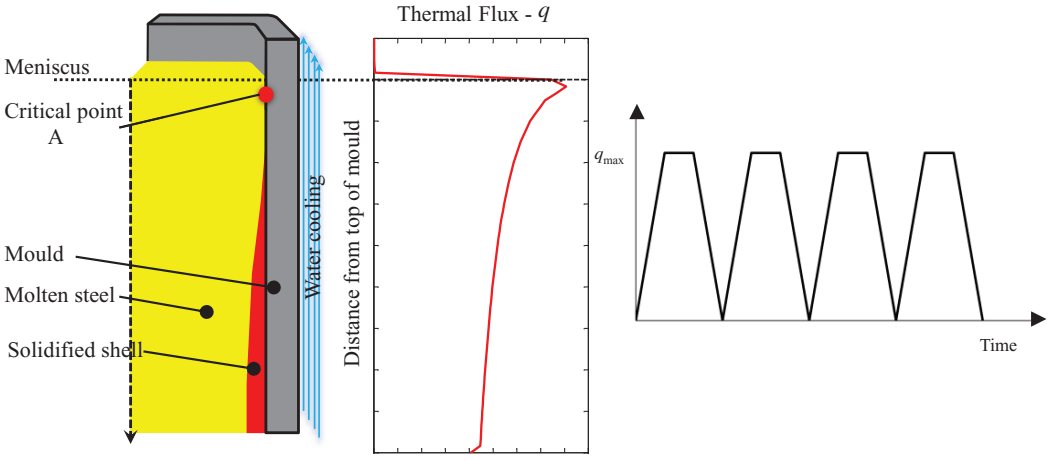

Fig. 1. Schematic description of the mould working conditions.

3. Nonlinear hardening models: theoretical background

Due to cyclic variation of the thermal flux, the mould is subjected to high temperature gradient which causes high thermal stresses, as well as plastic strains. Cyclic softening/hardening behaviour of the mould material can be captured by a combined kinematic and isotropic material model (see Fig. 2.):

$$f = \sqrt{\frac{3}{2}(\boldsymbol{\sigma}' - \boldsymbol{\alpha}') : (\boldsymbol{\sigma}' - \boldsymbol{\alpha}')} - R - \sigma_0 = 0 \tag{1}$$

where $\boldsymbol{\sigma}'$ and $\boldsymbol{\alpha}'$ are the stress and back stress deviator tensor respectively, σ_0 is the initial yield stress and R is the drag stress. Kinematic part is controlled by $\boldsymbol{\alpha}$, while isotropic part is related to R. Increment of the back stress, $\mathrm{d}\boldsymbol{\alpha}$, is usually expressed as function of plastic strain, $\varepsilon_{\mathrm{pl}}$, and accumulated plastic strain, $\varepsilon_{\mathrm{pl,acc}}$. According to Chaboche's model, the relation is [3]:

$$\boldsymbol{\alpha} = \sum_i \boldsymbol{\alpha}_i \; ; \quad \mathrm{d}\boldsymbol{\alpha}_i = \frac{2}{3} C_i \mathrm{d}\boldsymbol{\varepsilon}_{\mathrm{pl}} - \gamma_i \boldsymbol{\alpha}_i \mathrm{d}\varepsilon_{\mathrm{pl,acc}} \tag{2}$$

where C is the initial hardening modulus and γ defines the rate at which hardening modulus starts to decrease as the plastic strain develops. Chaboche's model is a superposition of several nonlinear kinematic models. When i=1 the model is often referred to as Armstrong & Frederick; in addition, Prager's linear kinematic model is obtained when γ=0, therefore relation (2) can be written as:

$$\mathrm{d}\boldsymbol{\alpha} = \frac{2}{3} C_{\mathrm{lin}} \mathrm{d}\boldsymbol{\varepsilon}_{\mathrm{pl}} \tag{3}$$

The integration of Eq. (2) with respect to ε_{pl}, for uniaxial loading and for i=1, leads to:

$$\alpha = \psi\frac{C}{\gamma} + \left(\alpha_0 - \psi\frac{C}{\gamma}\right)\exp\left[-\psi\gamma\left(\varepsilon_{pl} - \varepsilon_{pl,0}\right)\right] \tag{4}$$

where ψ=±1 according to the direction of flow, and $\varepsilon_{pl,0}$ and α_0 are the initial values of plastic strain and back stress, respectively. For tension ψ=1 and considering zeros initial values of plastic strain and back stress, Eq. (4) becomes:

$$\sigma = \sigma_0 + \frac{C}{\gamma}\left[1 - \exp\left(-\gamma\varepsilon_{pl}\right)\right] \tag{5}$$

To estimate material parameters using cyclic stress-strain loops, it is necessary to use [3]:

$$\sigma_a = \sigma_0 + \frac{C}{\gamma}\tanh\left(\gamma\varepsilon_{pl,a}\right) \tag{6}$$

where σ_a is the stress amplitude and $\varepsilon_{pl,a}$ is the plastic strain amplitude. The evolution of the yield surface size is expressed by the isotropic hardening:

$$\mathrm{d}R = e\left(R_\infty - R\right)\mathrm{d}\varepsilon_{pl,acc} \tag{7}$$

where R_∞ is the saturation value of the yield surface, e is the speed of stabilization and $\varepsilon_{pl,acc}$ is the accumulated plastic strain. R_∞ can be either positive or negative, giving rise to cyclic hardening or softening, respectively. The relation between R and $\varepsilon_{pl,acc}$ is obtained after integration:

$$R = R_\infty\left[1 - \exp\left(-e\varepsilon_{pl,acc}\right)\right] \tag{8}$$

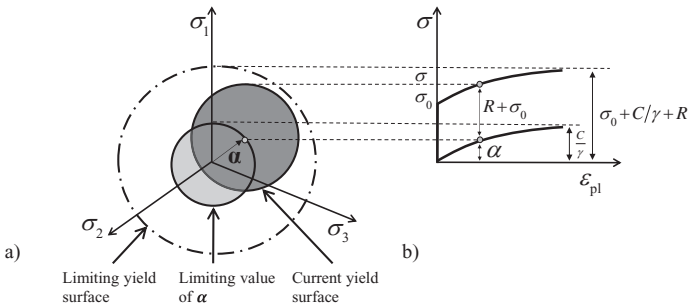

Fig. 2. Schematic evolution of the combined material model: a) in stress space and b) in uniaxial tension.

4. Calibration of material models

Isothermal low cycle fatigue tests were performed to characterize cyclic stress-strain behavior and fatigue strength of CuAg alloy at 20 °C, 250 °C and 300 °C. Performed tests were strain controlled with a strain ratio R_ε=-1. Stress-strain loops were recorded during the test for each cycle. Tests were interrupted before specimen failure when the maximal stress decreased by 80%.

The Young's modulus and the yield stress are firstly determined as they define the elastic region. The Young's modulus is determined by using both the tensile portion of the first hysteresis loop, E_1, and the stabilized loop, E_s. As shown in Table 1, the Young's modulus is a function of the temperature and it also seems to depend on the applied strain amplitude ε_a. Furthermore, the Young's modulus seems to slightly decrease during the applied cyclic loading.

Table 1. Estimated values of the Young's modulus.

Temperature	ε_a=0.3%		ε_a=0.4%		ε_a=0.5%		ε_a=0.7%	
	E_1 (MPa)	E_s (MPa)	E_1 (MPa)	E_s (MPa)	E_1 (MPa)	E_s (MPa)	E_1 (MPa)	E_s (MPa)
20 °C	119700	116900	119900	115900	118200	113500	118800	114900
250 °C	108500	93760	108600*	98530*	105400	90140	103900	85100
300 °C	105600	97930	104300	98820	101900	95770	103400	87690

*ε_a=0.35%

The initial yield stress, σ_0, is identified as a point on the tensile portion of the first hysteresis loop where plastic strain occurs; the actual yield stress, σ_{0*}, is measured by using the stabilized loop. The evolution of the yield stress with increasing number of cycles enables to determine the hardening or softening characteristics of the material, as can be seen in Table 2. In all evaluated cases $\sigma_{0*} < \sigma_0$, which confirms a softening behavior of the material.

Table 2. Estimated values of the yield stress.

Temperature	ε_a=0.3%		ε_a=0.4%		ε_a=0.5%		ε_a=0.7%	
	σ_0 (MPa)	σ_{0*} (MPa)	σ_0 (MPa)	σ_{0*} (MPa)	σ_0 (MPa)	σ_{0*} (MPa)	σ_0 (MPa)	σ_{0*} (MPa)
20 °C	121.64	87.95	138.76	91.44	117.97	84.25	154.94	114
250 °C	111.34*	51.71*	103.46	50.86	140.31	50.98	80.68	53.47
300 °C	124	44.7	103.3	48.23	116.37	40.49	122.5	43.48

*ε_a=0.35%

Once the Young's modulus and yield stress values are determined, nonlinear kinematic hardening material parameters, C and γ can be estimated. Material parameters are estimated using only the plastic regions of each stabilized cycle obtained under imposed ε_a. For a given stress-strain loop, the stress amplitude, σ_a, the plastic strain amplitude, $\varepsilon_{pl,a}$, and the actual yield stress, σ_{0*}, are measured at a stabilized cycle (half-life cycle) and plotted as in Fig. 3. a). The procedure is repeated at each strain amplitude. Eq. (6) is fitted to the measured points to obtain material parameters C, γ. The same fitting procedure is applied on experimental data obtained at different temperatures. Fig. 3. b) shows the good agreement between experimental and simulated stress-strain loop. Material parameter C_{lin} (Prager's model) is estimated by using a linear fitting for the plastic region of each stabilized cycle.

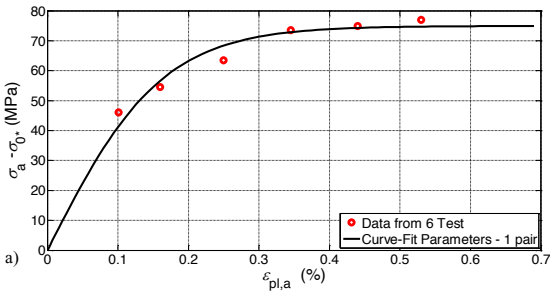

Fig. 3. a) Curve fitting by the method of least squares, using data of 6 hysteresis loops (T=20 °C);

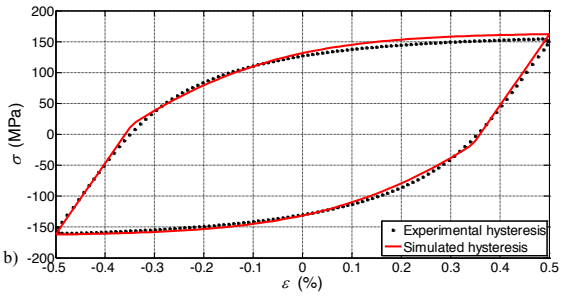

b) Comparison between experimental (ε_a=0.5%, T=20 °C) and simulated curves.

Nonlinear isotropic parameters are then estimated. The maximum stress, σ_{max}, is measured for each stress-strain cycle and plotted against the number of applied cycles, N, see Fig. 4. a), showing a softening behavior. The procedure is repeated for each imposed strain amplitude and temperature. The saturation stress, R_∞, is determined as the difference in the maximum stress of the first cycle, $\sigma_{max,1}$, and the stabilized one, $\sigma_{max,s}$. As can be noticed in Fig. 4. a), the saturation stress, R_∞, depends also on the applied strain amplitude, contrary to the assumption of the nonlinear isotropic model in Eq. (8). For each temperature an average R_∞ is calculated, see Table 3. The speed of stabilization, e, is estimated using the relation proposed by [3]:

$$\frac{\sigma_{\max,i}-\sigma_{\max,1}}{\sigma_{\max,s}-\sigma_{\max,1}} \approx \frac{R}{R_\infty} = 1-\exp\left(-e\varepsilon_{pl,acc}\right) = 1-\exp\left(-2e\Delta\varepsilon_{pl}N\right) \tag{9}$$

where $\sigma_{max,i}$ is the current maximum stress for the N^{th} cycle. Eq. (9) is shown in Fig. 4. b). A reasonable correlation is obtained, although a modification of the evolution rule of R seems necessary. Estimated material parameters used in numerical simulations are shown in Table 3.

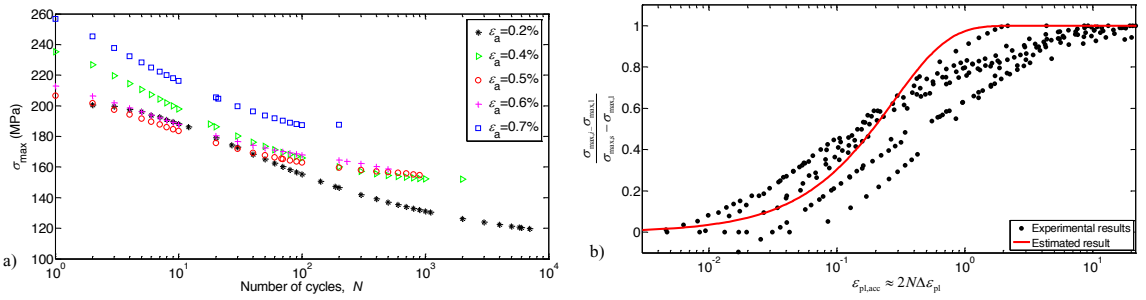

Fig. 4. a) Stress amplitude versus number of cycles (T=20 °C); b) The determination of the isotropic parameter e.

Table 3. Estimated material parameters used in numerical simulations.

Temperature	E (MPa)	E_s (MPa)	σ_0 (MPa)	σ_{0*} (MPa)	C (MPa)	γ	R_∞ (MPa)	e	C_{lin} (MPa)
20 °C	119080	110900	130	74	46250	617.2	-72.3	2.352	37439
250 °C	106600	94758	113	50	45340	820.9	-80.2	3.894	18039
300 °C	103800	94792	110	45	40080	832.8	-76.6	5.293	18466

5. Numerical simulations

A three dimensional (3D) finite element model is used as it allows one to represent a non-uniform distribution of the thermal flux through the length. The finite element model has a refined mesh in the meniscus region (see Fig. 5. a) where the highest thermal flux occurs. The model has two planes of symmetry, a total of 57024 elements and 63973 nodes.

A thermo-mechanical numerical analysis is performed. In the thermal analysis 8-node brick thermal elements are used (SOLID70 in ANSYS). Thermal flux is imposed on the inner surface of the model, while convection is considered on the outer surface to simulate water cooling. The temperature of the cooling water is 40 °C and the convection coefficient is 48000 W/m^{2}K. In thermal analysis, the variation of the thermal flux in Fig 1. is simulated by a sequence of steady state analysis. A nonlinear solution is carried out to simulate the temperature dependence of thermal properties.

The temperature distribution obtained from the thermal analysis is the input data for the mechanical simulation. In the mechanical simulation 8-node brick mechanical elements are used (SOLID185 in ANSYS). Furthermore, no mechanical constraints are imposed as the model is free to expand. A pressure of the molten steel, which acts on the

inner mould surface, is very small and then it was not considered in simulation. Temperature dependence of material parameters is also taken into consideration.

Different material models are considered and compared:

- Linear kinematic model
- Combined model (nonlinear kinematic + nonlinear isotropic)
- Stabilized model
- Accelerated model

The approximate number of cycles needed to reach stabilized conditions can be calculated by the relation $2eN\Delta\varepsilon_{pl}\approx 5$ proposed in [4]. The relation states that a value near 5 is a good saturation criterion. In the case of the combined material model, for $\Delta\varepsilon_{pl}=1.06\text{x}10^{-5}$ as calculated by FEM and $e=3.894$ it would be necessary to simulate roughly $N=60\ 567$ cycles to reach a stabilized stress-strain cycle. Simulation of such huge number of cycles requires unfeasible computational effort and time. Instead, the accelerated material model takes the rapidity of stabilization into consideration. By increasing the coefficient e, it is possible to reach stabilized stress-stain cycle with a smaller number of cycles. For example, with a larger value $e=100$, stabilization would be reached in 20 cycles. The stabilized material model instead is considered to be when R reaches R_{∞}. Material parameters C and γ used in stabilized model are the same as in the previous models, but in this case the parameters E and σ_0 are replaced by E_s and σ_{0*}, which correspond to the stabilized cycle.

The temperature distribution obtained at the maximum thermal flux, q_{max}, is shown in Fig 5. b). The maximum temperature appears near the meniscus area (point A) where also the highest thermal gradient across the thickness occurs, causing high thermal stresses. Fig 5. c) shows von Mises stress distribution at the q_{max} calculated by the combined material model. The most critical point A in the model is located 30 mm below the meniscus level.

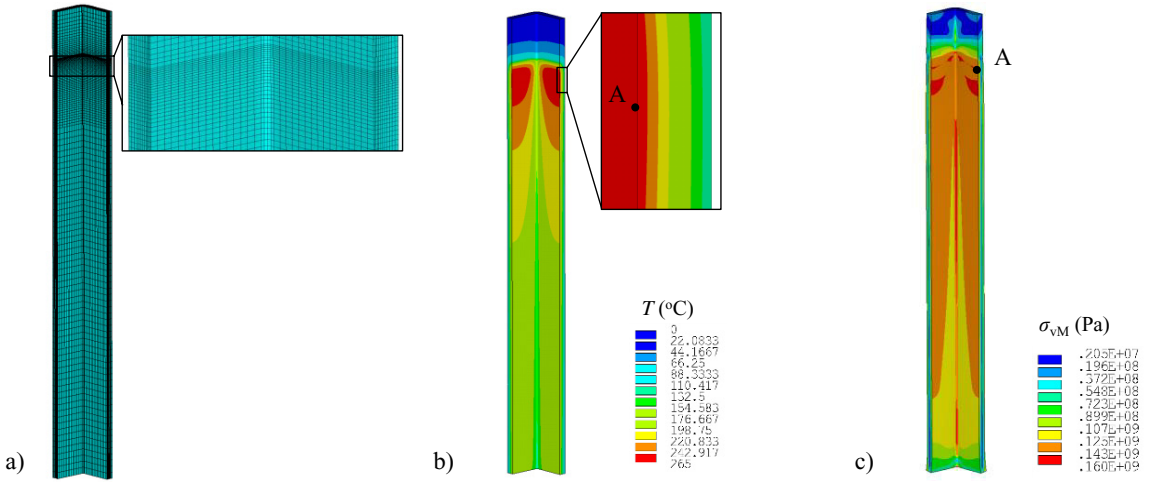

Fig. 5. a) 3-D finite element model; b) Temperature distribution at q_{max}; c) von Mises stress distribution.

Mechanical analysis simulates just 20 cycles. Fig. 6. shows the evolution during 20 cycles of the "hoop" stress-strain measured at the critical point A by using various material models defined before. The "hoop" component is parallel to the mould inner surface. In the first cycle, the temperature of the component increases, consequently compressive stresses appear because the lateral thermal expansion is constrained. Plastic strains occur because the developed compressive stresses exceed the yield stress. Using stabilized material model, yielding occurs at lower stress in the first cycle. Tensile stresses appear during the cooling phase. Depending on the type of the material model, elastic or elasto-plastic behavior is observed in successive cycles. For example, combined material model shows a predominant elastic behavior. Consequently, the nonlinear isotropic softening material model, which is dependent on plastic strain, has slight influence on the behavior of combined model. Therefore a huge number of

cycles have to be simulated to reach the stabilized stress-strain state. The stabilized model instead shows an elasto-plastic behavior.

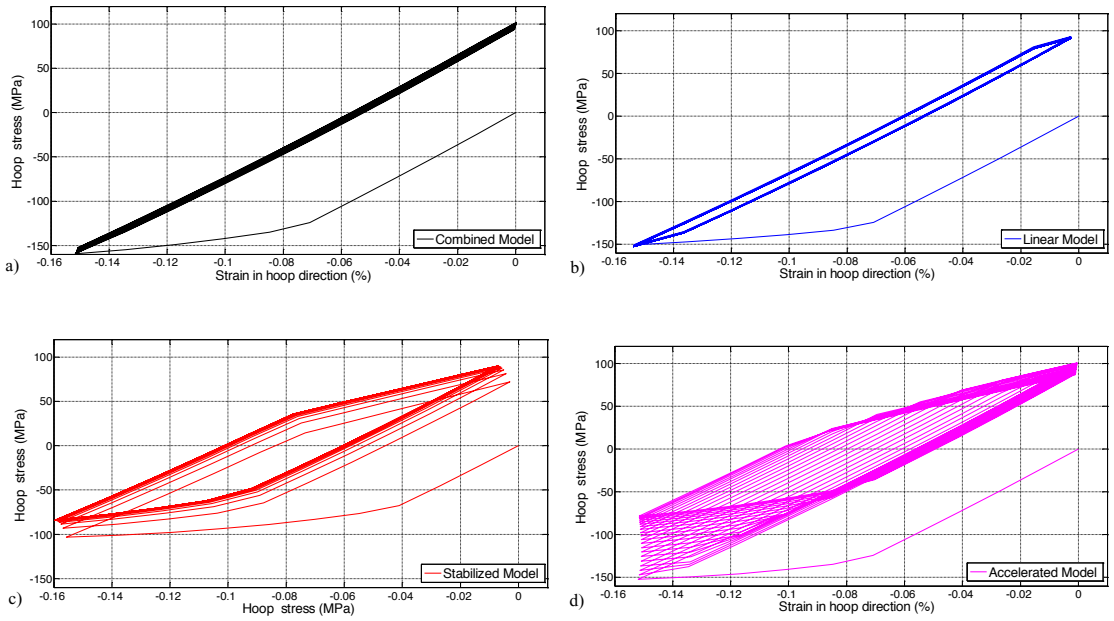

Fig. 6. Cyclic "hoop" stress-strain evolution for different material models.

6. Fatigue life assessment

The fatigue life of the copper mould is now estimated by considering the critical point A. Both elastic, ε_{el}, and plastic strains, ε_{pl}, appears in the critical point A, therefore strain-based fatigue approach can be used. Firstly Manson-Coffin-Basquin equation is used to relate strain and number of cycles to failure:

$$\frac{\Delta\varepsilon}{2}=\frac{\Delta\varepsilon_{el}}{2}+\frac{\Delta\varepsilon_{pl}}{2}=\frac{\sigma'_f}{E}\left(2N_f\right)^b+\varepsilon'_f\left(2N_f\right)^c \tag{10}$$

where σ'_f, b, ε'_f, c are four parameters estimated from isothermal LCF data, see Table 4. Estimation of the parameters is performed by applying least square fitting method.

Table 4: Estimated material parameters for Manson-Coffin-Basquin method.

Temperature	σ'_f (MPa)	b	ε'_f	c
20 °C	359.1	-0.1031	0.07689	-0.3942
250 °C	253.6	-0.1018	0.2942	-0.5311
300 °C	240.4	-0.1068	0.4258	-0.5708

An alternative method, which relates strain and cycles to failure, is the Universal Slopes equation, which assumes that the elastic and the plastic lines have unique slopes (0.12 and 0.6, respectively) for all materials:

$$\Delta\varepsilon=\Delta\varepsilon_{el}+\Delta\varepsilon_{pl}=3.5\frac{\sigma_{uts}}{E}N_f^{-0.12}+D^{0.6}N_f^{-0.6} \tag{11}$$

where σ_{uts} is the ultimate tensile strength and D is the ductility, which is related with the area reduction in a tensile test. Ultimate strength, ductility and Young's modulus can be determined using tensile test data. Although originally proposed for steel [5], the Universal Slopes equation is applied and compared here to the experimental data of a copper alloy. The Universal Slopes equation applies at room temperature. However, creep and high temperatures are known to reduce up to 90% of fatigue life [5]. A rough estimate is provided by 10% Rule as suggested in [5]. The 10% Rule estimates that, at the high temperatures, only 10% of the life computed by the Universal Slopes equation will actually be achieved. The Universal Slopes equation gives the upper bound life, while the 10% Rule gives the lowest expected life i.e. lower bound life. The average mean fatigue life is estimated to be twice of the lower bound (20%), as suggested by [5]. Finally, an equivalent strain range has to be calculated to apply the strain life equation when the stress is multiaxial:

$$\Delta\varepsilon_{eq} = \frac{\sqrt{2}}{3}\sqrt{\left[\Delta(\varepsilon_1-\varepsilon_2)\right]^2+\left[\Delta(\varepsilon_2-\varepsilon_3)\right]^2+\left[\Delta(\varepsilon_3-\varepsilon_1)\right]^2} \tag{12}$$

where $\Delta(\varepsilon_i-\varepsilon_j)$ is the range of the difference between principal strains. Consequently, the elastic part in Eq. (10) and (11) must be shifted downward as suggested in [6]. Final relations for the Manson-Coffin-Basquin and the Universal Slopes equation are:

$$\frac{\Delta\varepsilon_{eq}}{2} = \left[\frac{2}{3}(1+\nu)\right]\frac{\sigma'_f}{E}(2N_f)^b + \varepsilon'_f(2N_f)^c \tag{13}$$

$$\Delta\varepsilon_{eq} = \left[\frac{2}{3}(1+\nu)\right]3.5\frac{\sigma_{uts}}{E}N_f^{-0.12} + D^{0.6}N_f^{-0.6} \tag{14}$$

Material parameters estimated at 20 °C are used to obtain the fatigue curve defined by the Universal Slopes equation. The Manson-Coffin-Basquin curve is obtained using experimental data at 250 °C. Fig. 7. shows the Manson-Coffin curve and the Universal Slopes (upper bound life); the figure also shows the curve for the 10% Rule (lower bound) and the 20% Rule (average). It is worth noting how the Universal Slopes equation tends to be slightly under conservative compared to the experimental data at 250 °C, while the 10% Rule curve seems to be over conservative, at least for this alloy at this temperature.

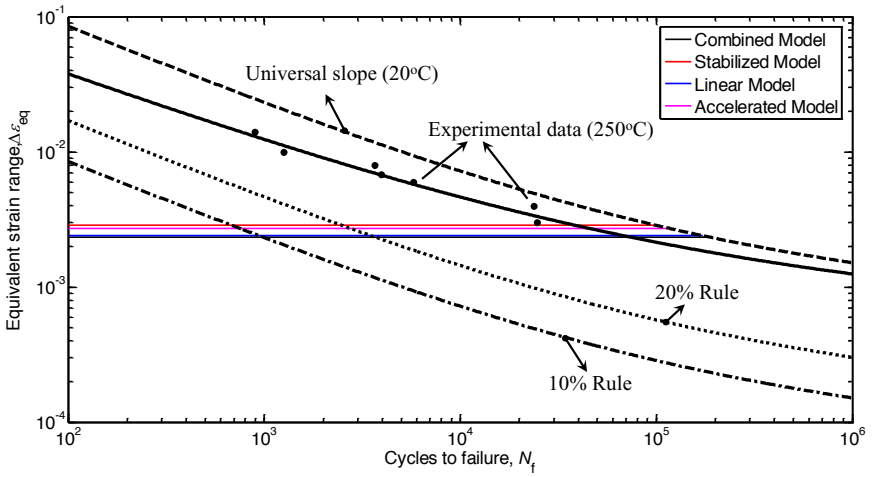

Fig. 7. Equivalent strain range versus number of cycles to failure.

The fatigue life at the most critical point A is calculated with different material models used in simulations and depending on different fatigue curves, see Table 5. The results show that similar fatigue lives are obtained by combined and linear kinematic material models, regardless of the fatigue curve. This is due to the fact that, as the combined material model requires 60547 cycles to reach stabilized stress-strain state, its response after 20 cycles is almost similar to that of the linear kinematic one. On the other hand, in the stabilized material model, due to the lower yield stress, σ_{0*}, in the first cycles plasticization phenomena area enhanced. In fact, in [7], it was observed that direct use of the stabilized model could leads to heavy mistakes, especially in the case of softening materials. Therefore, the accelerated material model seems to be a good compromise among the previously discussed approaches. In particular, it can be noticed from Table 5 that the accelerated model gives the lowest value of fatigue life, confirming that the method has to be adopted also according to a safe engineering design point of view.

Table 5: Estimated fatigue life for the critical point A.

Material Models	$\Delta\varepsilon_{eq}$	Number of cycles to failure			
		Experimental curve	Universal Slopes	10% Rule	20% Rule
Combined Model	0.00234	74623	188484	993	3711
Stabilized Model	0.00287	38511	99769	680	2473
Linear Model	0.00240	68839	173475	948	3512
Accelerated Model	0.00270	46737	118870	760	2788

7. Conclusions

A thermo-mechanical analysis of a copper mould for the continuous steel casting is described in this work. Several material models are studied and compared. Material parameters were estimated for CuAg alloy in the temperature range between 20 ^{o}C and 300 ^{o}C. The equivalent strain range was then calculated for the most critical point A located in the model. As a final result, the service lives estimated by different material models and fatigue life models are compared. The combined nonlinear kinematic and isotropic material model requires huge computational time to reach a stabilized stress-strain loop. On the other hand the use of the stabilized model overestimates the plasticization phenomena already in the first cycle. An alternative accelerated material model, where stabilization is reached earlier, is thus proposed, proofing that it is able to give suitable and safe life estimation for design purposes.

References

[1] J.K. Park, B.G. Thomas, I.V. Samarasekera, U.S. Yoon, Thermal and Mechanical Behavior of Copper Molds during Thin-Slab Casting (II): Mold Crack Formation, Metallurgical and Materials Transactions B, 33B (2002) 437-449.
[2] J.K. Park, B.G. Thomas, I.V. Samarasekera, U.S. Yoon, Thermal and Mechanical Behavior of Copper Molds during Thin-Slab Casting (I): Plant Trial and Mathematical Modeling, Metallurgical and Materials Transactions B, 33B (2002) 1-12.
[3] J. Lemaitre, J.L. Chaboche, Mechanics of solid materials, Cambridge University Press, Cambridge, 1990.
[4] J.L.Chaboche, A review of some plasticity and viscoplasticity constitutive theories, International Journal of Plasticity, 24 (2008) 1642-1693.
[5] S. S. Manson, A Simple Procedure for Estimating High-temperature Low-cycle Fatigue, Experimental Mechanics, 8 (1968) 349-355.
[6] S. S. Manson, Thermal Stress and Low-cycle fatigue, McGraw-Hill, 1966.
[7] J.L.Chaboche, G. Cailletaud, On the calculation of structures in cyclic plasticity or viscoplasticity, Computers & Structures, 23 (1986) 23-31.